ACS APPLIED MATERIALS & INTERFACES

Research Article

www.acsami.org

# Sodium Titanate Nanotubes as Negative Electrode Materials for Sodium-Ion Capacitors

Jiao Yin,[†,‡] Li Qi,[†] and Hongyu Wang*[,†]

[†]State Key Laboratory of Electroanalytical Chemistry, Changchun Institute of Applied Chemistry, Chinese Academy of Sciences, 5625 Renmin Street, Changchun 130022, China

[‡]Graduate School of Chinese Academy of Sciences, Beijing 100039, China

Supporting Information

**ABSTRACT:** The lithium-based energy storage technology is currently being considered for electric automotive industry and even electric grid storage. However, the hungry demand for vast energy sources in the modern society will conflict with the shortage of lithium resources on the earth. The first alternative choice may be sodium-related materials. Herein, we propose an electric energy storage system (sodium-ion capacitor) based on porous carbon and sodium titanate nanotubes (Na-TNT, $Na^+$-insertion compounds) as positive and negative electrode materials, respectively, in conjunction with $Na^+$-containing non-aqueous electrolytes. As a low-voltage (0.1−2 V) sodium insertion nanomaterial, Na-TNT was synthesized via a simple hydrothermal reaction. Compared with bulk sodium titanate, the predominance of Na-TNT is the excellent rate performance, which exactly caters to the need for electrochemical capacitors. The sodium-ion capacitors exhibited desirable energy density and power density (34 Wh $kg^{-1}$, 889 W $kg^{-1}$). Furthermore, the sodium-ion capacitors had long cycling life (1000 cycles) and high coulombic efficiency (≈ 98 % after the second cycle). More importantly, the conception of sodium-ion capacitor has been put forward.

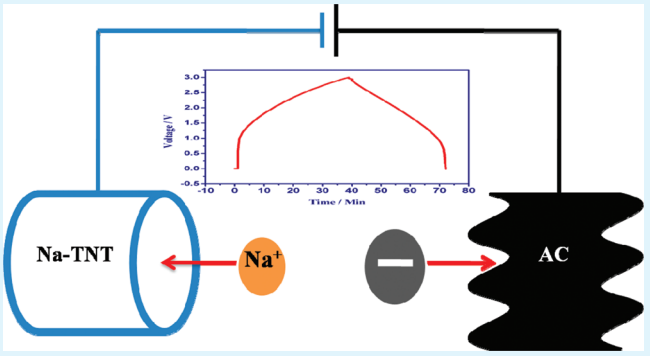


**KEYWORDS:** *sodium titanate, nanotubes, negative electrode, materials, sodium-ion, capacitors*

## 1. INTRODUCTION

Electrochemical capacitors (ECs) are considered as one of the most promising candidates for new-generation green energy storage devices in terms of their high power density, long cycle life, and desirable cycling stability.[1−3] Their energy density, however, is rather small compared with that of secondary batteries.[4] To solve this problem, asymmetric "hybrid" electrochemical capacitors (in short, hybrid capacitors) have been proposed by combining battery-type electrodes and capacitor-type electrodes (generally porous carbon) to make a compromise between the energy density and power density.[5−10] Especially, the hybrid capacitors using $Li^+$-based nonaqueous electrolytes appear the most prominent in terms of energy density. At first, their working voltages are quite high, for instance, they can reach 4 V in the case of lithium-ion capacitors (activated carbon/lithium-pre-doped carbon). Second, the charge storage quantity corresponding to $Li^+$ insertion into battery-type electrodes is overwhelmingly large in comparison with the double-layer capacitance of porous carbon electrode. However, just like the development consequence of Li-ion batteries, the hungry demand for vast energy sources in modern society will conflict with the shortage of lithium resources on the earth. Thus, it is an urgent task to explore alternative hybrid capacitors using abundant and economic materials. The most appealing alternative is to use sodium because its resources are in principle unlimited and very easy to renew.

Some recent studies have become interested in exploring $Na^+$-based technologies.[11] Most of them concentrated on positive electrode materials for Na-ion batteries.[12−18] Nevertheless, more recent computational studies have revealed that a wide variety of $Na^+$-related electrodes operate on voltages of 0.18−0.57 V lower than that of $Li^+$ analogues.[19,20] This means that the overall energy density of Na-ion batteries will be sacrificed to some extent if $Na^+$-related materials were utilized for the positive electrodes. On the contrary, some $Na^+$-related materials may be suitable for negative electrodes from the viewpoint of their low $Na^+$-insertion potential profiles.[21] Considering the above facts, we propose here an electric energy storage system based on porous carbon and $Na^+$-insertion compounds as the positive and negative electrode materials, respectively, in conjunction with $Na^+$-containing non-aqueous electrolytes. The employment of porous carbon can circumvent the embarrassment caused by $Na^+$-related positive electrode materials because the charge storage principle at the porous carbon electrode side only refers to the adsorption of

Received: March 1, 2012
Accepted: April 13, 2012
Published: April 13, 2012

   dx.doi.org/10.1021/am300385r | ACS Appl. Mater. Interfaces 2012, 4, 2762−2768

anions instead of $Na^+$ insertion. Then the problem shifts to the choice of satisfactory negative electrode materials.

Indeed, some efforts have been made to explore Na-ion battery negative materials. Graphite and Na metal have made us disappointed due to some unavoidable shortcomings.[19,22−24] Carbon materials have been testified as unsatisfactory candidates due to their high capacity fadings.[21,25−27] More recently, sodium insertion into bulk $Na_2Ti_3O_7$ at low voltage makes it possible for sodium titanates to be used as negative materials.[21] From the viewpoint of rate performance, the nanostructured electrode materials are preferred to bulk ones.[28−30] Among them, nanotubes stand out due to their large surface area, open tunnel structures, and short diffusion path for ion intercalation−deintercalation. Hydrothermal treatment of different $TiO_2$ precursors in concentrated NaOH is a facile and effective way to synthesize sodium titanate nanotubes (Na-TNTs). In this work, Na-TNTs were syntheiszed via a hydrothermal treatment of P25 (commercial $TiO_2$) with NaOH solution.[31−33] The structure and morphology of the heat treatment samples were detailedly investigated, and the electrochemical properties for sodium storage were fully studied. More importantly, sodium-ion hybrid capacitors based on AC and Na-TNTs were firstly proposed. The performance of sodium-ion hybrid capacitors is comparable to that of AC/$Li_4Ti_5O_{12}$ or graphite/$TiO_2$ hybrid capacitors using $Li^+$-based electrolytes.[5,34]

## 2. EXPERIMENTAL SECTION

**2.1. Synthesis of Na-TNTs.** P25 (commercial $TiO_2$ powder, which comprises of 25 % rutile and 75 % anatase, the particle size of P25 is about 30 nm). Na-TNTs were synthesized by a hydrothermal treatment of P25 with 10 M NaOH solution in a sealed Teflon-lined autoclave at 150 °C for 48 h.[31,38] The product from centrifugation was washed by deionized water until a pH value of 8 was accurately achieved. After being dried in an oven for 48 h (60 °C in air), the as-synthesized samples were carried out with heat treatment at different temperatures (300, 400, 500, and 600 °C in air, respectively) for 5 h. The samples were labeled as $T_0$ (as-prepared), $T_1$ (300 °C), $T_2$ (400 °C), $T_3$ (500 °C), and $T_4$ (600 °C), respectively. Furthermore, the samples washed with different pH values were also investigated (see Supporting Information). Finally, the bulk $Na_2Ti_3O_7$ and $Na_2Ti_6O_{13}$ were also investigated (see Supporting Information).

**2.2. Characterization Methods.** X-ray diffraction (XRD) characterization of the samples were operated on a Rigaku-Dmax 2500 diffractometer attached with graphite monochromatized Cu K$\alpha$ ($\lambda$ = 0.15405 nm) radiation at a scanning speed of 4°/min in the range from 2° to 90°. Transmission electron microscopy (TEM) was carried out with Hitachi model H-8100 operating at 200 kV accelerated voltage. Scanning electron microscopy (SEM) images were carried out by Philips XL 30 and JEOL JSM-6700F microscopes. Raman spectra of all samples were recorded by a Renishaw 2000 model confocal microscopy Raman spectrometer with a CCD detector and a holographic notch filter. Radiation of 514.5 nm from an air-cooled argon ion laser was employed for the Raman excitation.

**2.3. Fabrication of Electrodes.** The activated carbon (AC) electrode material used in this work was commercial activated carbon (from ShangHai Carbosino Material CO., Ltd.), with a specific surface area of 1800 $m^2\ g^{-1}$. The electrodes were prepared by pressing the mixture of active material (Na-TNTs or AC) and TAB (teflonized acetylene black) on each stainless steel mesh (1 $cm^2$ area). Finally, the electrodes were performed with dryness in a vacuum oven at 180 °C for 3 h before assembling.

**2.4. Electrochemical Measurements.** All the electrochemical tests were carried out with coin-type cells (CR2032). Na half-cells were assembled in the coin-type cells with a Na metal foil as the negative electrode, glass fiber separator, and 1.5 M $NaClO_4$ in an electrolyte mixture of PC and DMC (1:2 by vol). Half-cells were cycled galvanostatically at different currents between 2 and 0.1 V (vs $Na/Na^+$), respectively, using LAND-CT2001A tester at ambient temperature. Na ion full-cells were assembled in the same manner as half-cells with an AC cathode. Sodium ion full-cells were cycled galvanostatically at varying currents between 0−3 V or 0−2.5 V. All cell assembly operations were performed in an Ar-filled dry glovebox (M Braun, containing <1 ppm of $O_2$ and $H_2O$).

## 3. RESULTS AND DISCUSSION

**3.1. Compositions and Morphologies.** Figure 1A demonstrates the XRD patterns of all samples washed with a pH value of 8. For $T_0$, $T_1$, and $T_2$, the strong broad peaks around $2\theta$ = 9.6° are typical of layered titanates caused by the interlayer distance. The chemical formula of the $T_0$ sample is assigned as $Na_xH_{2-x}Ti_3O_7{\cdot}nH_2O$ ($0 < x < 2$, and $n < 1.2$) according to the XRD profile and reported literature.[35−39] After the heat treatment at 300 and 400 °C, the crystallinity of

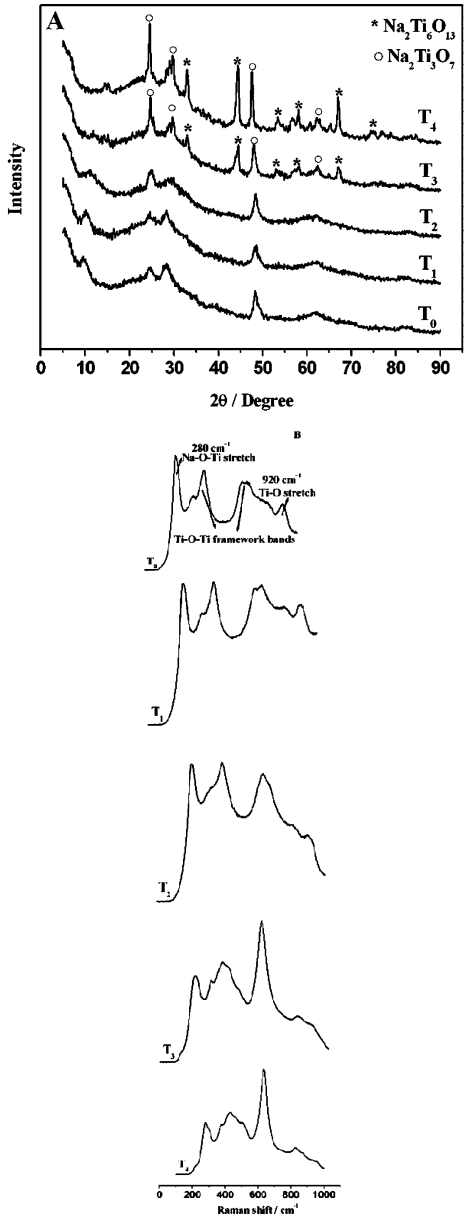


**Figure 1.** (A) XRD patterns of $T_0$ (the as-prepared sample), $T_1$ (300 °C), $T_2$ (400 °C), $T_3$ (500 °C), $T_4$ (600 °C). (B) Raman spectra of all samples ($T_0$, $T_1$, $T_2$, $T_3$, $T_4$).

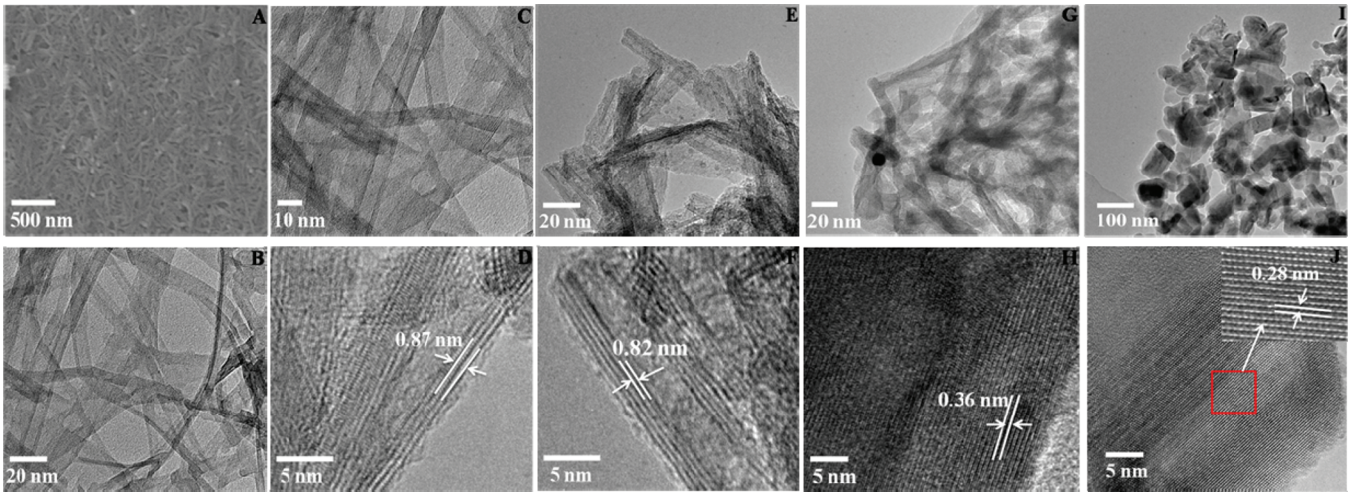


**Figure 2.** FE-SEM image of $T_0$ (A). TEM image of $T_0$ (B), $T_1$ (C), $T_2$ (E) and $T_3$ (G) and $T_4$ (I). HRTEM image of $T_1$ (D), $T_2$ (F), $T_3$ (H), and $T_4$ (J).

nanotubes is improved due to dehydration. However, the position of the diffraction peak at 9.6° shifts to a higher value (10.2°, 10.9°) with an increase of temperatures (≤ 400 °C), indicating the shrinkage of layered structure. This is attributed to the releasing of the water molecules confined in the interlayer.[27,35] The chemical formula of $T_1$ and $T_2$ is attributed to $Na_xH_{2-x}Ti_3O_7$ ($x > 1$) estimated by TGA, XPS, and EDX.[27,35] Nevertheless, we find that at 500 °C, the XRD pattern begins to be changed with an obvious shift of the first diffraction peak to higher $2\theta$ (shorter interlayer distance) and some new peaks emerge besides $Na_2Ti_3O_7$. This phenomenon is really owing to the transformation of the nanotube crystal structure and the new phase is $Na_2Ti_6O_{13}$.[39,40] After the calcination at 600 °C, the intensity of the representative peaks of $Na_2Ti_6O_{13}$ is strengthened due to complete dehydration. To further confirm their compositions, Figure 1B exhibits the Raman spectra measurments for all samples. The two typical broad bands for the as-synthesized and calcined products at 280 and 920 $cm^{-1}$ stand for the Na−O−Ti stretching vibration and the stretching vibration mode of short Ti−O bonds which refer to the nonbridging oxygen linked with sodium ions, respectively.[33−36] It was reported that the peaks for the two bands (280 and 920 $cm^{-1}$) are characteristic for sodium titanates and it cannot be observed for hydrogen titanates.[33−36] In conclusion, the Raman measurements further indicate that all the products are sodium titanates. It could be observed that no anatase and rutile phases appear during the calcination process.

To further investigate the influences of heat treatment on structure and morphology of Na-TNTs, parts A and B of Figure 2 show the SEM and TEM of $T_0$. Parts C−J of Figure 2 show the TEM and HRTEM of $T_1$, $T_2$, $T_3$, and $T_4$, respectively. The as-prepared Na-TNTs are several tens to hundred nanometers and are all open at both ends. The diameters of nanotubes are about 6−10 nm. After the heat treatment at 300 and 400 °C, the crystallinity of nanotubes is improved due to dehydration. The calcined samples maintain the tubular and multilayered morphology, and the interlayer distances are about 0.87 and 0.82 nm, respectively. When the as-synthesized Na-TNTs had undergone heat treatment at 500 °C, the product still retains the tubular structure with good crystallinity. The interlayer distance is reduced to 0.36 nm, which is ascribed to the crystal structure of $Na_2Ti_6O_{13}$. However, the hollow tube-like morphology completely disappears after heat treatment at 600 °C in air. The structure observed from TEM, indeed, becomes nanorods at 600 °C and the crystallinity is dramatically improved due to complete dehydration. The diameters of the solid nanorods are enlarged, typically between 20 and 50 nm. The interlayer space is dropped to 0.28 nm, which is also attributed to the crystal structure of $Na_2Ti_6O_{13}$. In conclusion, the morphology observed from our study is consistent with previous literature.[26,39,40]

**3.2. Electrochemical Performance.** The sodium ion insertion−deinsertion behaviors of all calcined samples were investigated by galvanostatic charge−discharge cycling measurements. The initial charge−discharge curves of the calcined products at the current density of 0.17 A $g^{-1}$ are presented in Figure 3A. It reveals that the potential plateaus, indeed, are much lower than that of Li analogues. As a result, the Na-TNT can be used as negative material for sodium ion hybrid energy devices. The initial discharge capacities are 152 and 144 mAh $g^{-1}$ for $T_1$ and $T_2$, respectively. However, the initial discharge capacities drop dramatically to 65 and 46 mAh $g^{-1}$ for $T_3$ and $T_4$, respectively. The irreversible capacities of the four nanotubes in the first cycle are 34, 41, 25, and 26 mAh $g^{-1}$, respectively. The coulombic efficiency decreases from 77.7 to 71.5, 63.1, and 45.7 %, respectively. For comparison, the sodium storage properties of samples washed with different pH values were also studied. However, we found that the samples washed with low pH values (5 and 7) are not stable during the high-temperature heat treatment and will be dehydrated and become more stable $TiO_2$.[31−36] Thus we mainly focused on comparing the performance of sodium storage for the samples calcined at low temperature (400 °C). The initial discharge curves of the products washed with different pH values (calcined at 400 °C) were displayed in Supporting Information Figure S1. It reveals that the discharging capacities of samples rank as follows: pH = 8 > pH = 9 > pH = 7 > pH = 5. The possible explainations are listed as follows. It was reported that the washing conditions of the as-prepared samples have a big influence on the compositions and microstructure of resultant products.[35,40] The samples washed with lower pH values possess the lower sodium content. Nevertheless, the higher sodium content is favorable to maintain the original

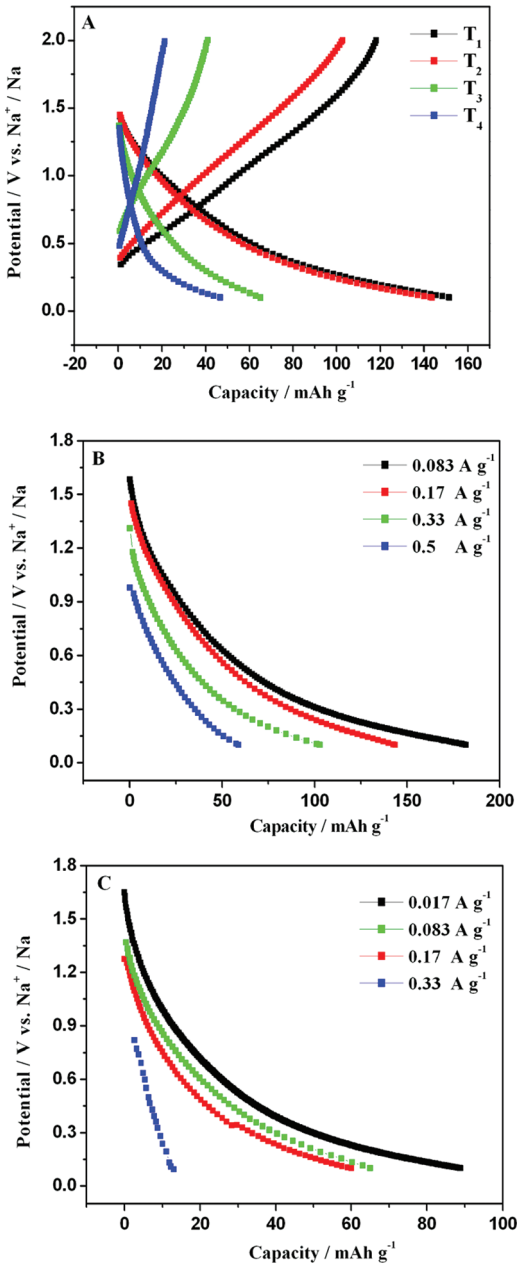


**Figure 3.** (A) Initial charge–discharge curves for calcined samples ($T_1$, $T_2$, $T_3$, $T_4$) between 0.1 and 2 V at the current density of 0.17 A $g^{-1}$. The first discharge curves for $T_2$ (B) and $T_3$ (C) between 2 and 0.1 V at different current density.

compositions and microstructure during the heat treatment.[35,40] The lower pH values of samples lead to poor stability and disappearance of multilayered nanotubes as the sample undergoes calcination.[35,40] As a result, the sample with a pH value of 5 possessed the lowest discharge capacity because its original composition is very close to $H_2Ti_3O_7$, which easily decomposes as $TiO_2$ during the heat treatment.[35,40] As for the sample washed with a pH value of 7, the lower discharge capacity results from the reduced interlayer distance as the $Na^+$ locating in the interlayer were gradually exchanged by $H^+$ during the washing process. However, the sample washed with a pH value of 9 possessed the highest sodium content, which is adverse for sodium ions in electrolyte to insert and deinsert as the interlayer space is occupied by excessive $Na^+$ sitting in the interlayer. Hence, the discharge capacity was also not high. The sample washed with a pH value of 8 has an appropriate sodium content to maintain its broad interlayer space and has little influence on sodim insertion–deinsertion. Consequently, its discharge capacity is somewhat larger than that of other samples. In addition, the galvanostatic charge–discharge experiments for the bulk $Na_2Ti_3O_7$ and $Na_2Ti_6O_{13}$ were also carried out. They delivered certain discharge capacities at very low current density (6.8 mA $g^{-1}$), which is accordant with the results obtained by Senguttuvan et al.[21] At high current density, the bulk $Na_2Ti_3O_7$ and $Na_2Ti_6O_{13}$ cannot exhibit discharge capacity (the data is shown in Supporting Information Figure S2). There are two main reasons for Na-TNTs calcined at low temperatures to have larger reversible capacities and higher coulombic efficiency than that of samples calcined at high temperatures. The first is the interlayer spacing differences of Na-TNTs calcined at different temperatures. The water molecules confined in the interspace of layers cannot be completely removed for the samples calcined at low temperatures, which also contributed to maintaining the large interlayer distance of tubes. Hence, the interlayer distances of $T_1$ and $T_2$ are much larger than that of $T_3$ and $T_4$, which could facilitate the larger-sized sodium ion (ionic radii of 102 pm) insertion–deinsertion into/from the layered crystal structure at high current density. Second, the high specific surface area of the nanotube could provide efficient contact between the Na-TNT and the nonaqueous electrolyte, and the thin diameter of the Na-TNT can reduce the distance of sodium ion diffusion in the nanotube electrodes. In addition, the capacity retention at high current density was investigated, which is consistent with above inferences. $T_1$ and $T_2$ possess certain capacity retention at high current density. $T_3$ and $T_4$ cannot sustain fast charge–discharge tests. The voltage profiles of $T_2$ and $T_3$ for charging to 2 V and discharging to 0.1 V at increasing charge–discharge current density from 0.017 to 0.5 A $g^{-1}$ are demonstrated in parts B and C of Figure 3, respectively. They demonstrate that the smaller-sized Na-TNT can sustain fast charge and discharge measurements. However, the cell voltages decrease with the increasing current density, which could be mainly attributed to the low conductivity of Na-TNT and the difficulty for larger-sized $Na^+$ insertion and deinsertion at high rates. In addition, the long cycling performance of all calcined samples are displayed in Supporting Information Figure S3, which indicates that the samples exhibit high capacity retention after 50 cycles (vs $Na/Na^+$). Among these samples, $T_2$ was preferential selected as negative material to assemble hybrid capacitor with AC in terms of the stability during the process of charge–discharge cycling tests (vs $Na/Na^+$) as $T_2$ possesses better crystallinity than that of $T_1$.

The capacitor voltage plays an important role in improving both the capacitor's energy density and power density. The working voltages of both symmetrical and asymmetrical capacitors were obtained according to their half-cell voltages vs $Na/Na^+$ during the process of galvanostatic charge–discharge tests. Parts A and B of Figure 4 show the plots of voltage versus time for AC/Na-TNT and AC/AC capacitors at the current density of 0.17 A $g^{-1}$. The overall operating voltage of the hybrid capacitor (AC/Na-TNT) can reach to 3 V, which is higher than that of the symmetrical AC/AC capacitor (2.5 V). This voltage enhancement could attribute to the difference of their half-cell voltage ranges (vs $Na/Na^+$). For the Na-TNT electrode, the voltage range for sodium intercalation reaction occurring at the Na-TNT negative electrode located between 0


dx.doi.org/10.1021/am300385r | ACS Appl. Mater. Interfaces 2012, 4, 2762–2768

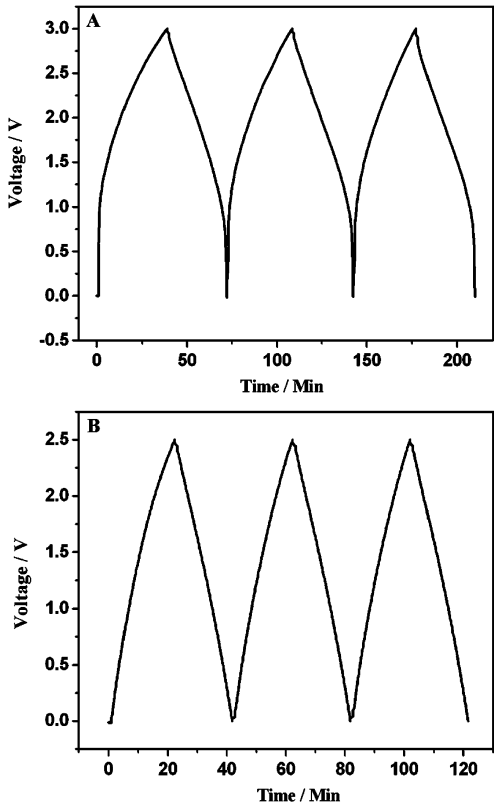


Figure 4. Representative galvanostatic charge−discharge curves of AC/Na-TNT (A) and AC/AC (B) capacitors at a current density of 0.17 A $g^{-1}$.

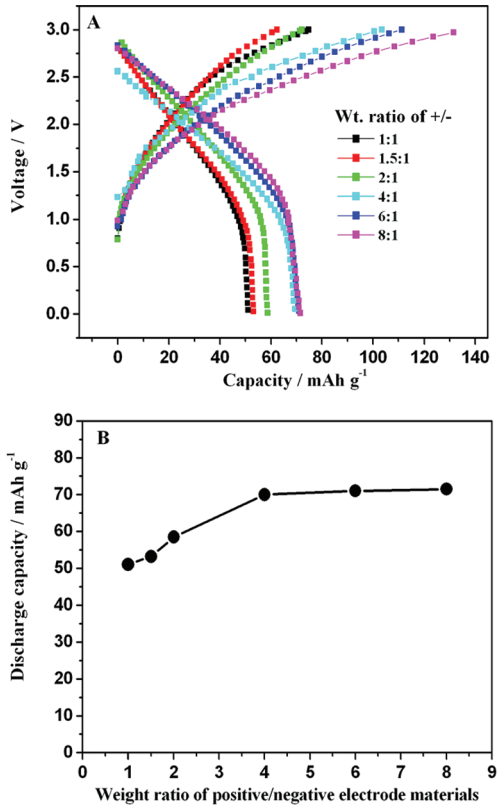


Figure 5. (A) Initial charge−discharge curves of AC/Na-TNT capacitors at different weight ratios of positive/negative electrode materials. (B) Relationship between the initial discharge capacity and the weight ratio of positive to negative electrode materials in AC/Na-TNT capacitors.

and 2 V (vs $Na/Na^+$). For the AC negative electrode, the voltage range located between 0 and 1.5 V (vs $Na/Na^+$). As a result, the overall working voltage range can be obtained from their overlapped cyclic voltammograms with AC positive electrode. Furthermore, the shapes of the charge−discharge curves of the hybrid capacitor are bent curves instead of straight lines and the discharge capacity dropped sharply at low voltage for the reason that the intercalation of sodium ion occurs at low potential portions (vs $Na/Na^+$) for Na-TNT.

It was reported that the match between positive and negative electrode has a big influence on the overall performance (such as operating voltage, cycling performance, capacity retention, coulombic efficiency, energy density, and power density) of hybrid electrochemical capacitors because of adopting various types of electrode materials.[41,42] Figure 5A demonstrates the first galvanostatic charging−discharging cycle curves of AC/Na-TNT capacitors at various weight ratios ($m^+$:$m^-$). Figure 5B shows the changes of initial discharge capacities for different AC/Na-TNT capacitors with the increase of weight ratio between positive and negative electrode. The curves reveal that the discharge capacity increases with enhanced weight ratio of positive/negative electrode materials. The discharge capacity in AC/Na-TNT capacitors manifest saturated value as the weight ratios ($m^+$:$m^-$) become very large. From the previous investigation,[41,42] the saturated value of discharge capacity in AC/Na-TNT capacitors can be acquired. Hence, the optimized weight ratio between positive and negative electrode ($m^+$:$m^-$ = 4:1) can be achieved on the basis of the overall performance of hybrid capacitors.

To compare the energy density and power density of symmetrical AC/AC and asymmetrical AC/Na-TNT electrochemical capacitors, the Ragone plots of two capacitors are displayed in Figure 6A. The energy density and power density were obtained from the galvanostatic discharge test curves by adding up the overall mass of both electrode active materials. The asymmetrical AC/Na-TNT capacitor has both higher energy density and power density (34 Wh $kg^{-1}$, 889 W $kg^{-1}$) than that of the symmetrical AC/AC capacitor (26 Wh $kg^{-1}$, 315 W $kg^{-1}$). Furthermore, the long cycling performance of the hybrid AC/Na-TNT electrochemical capacitor at the current density of 0.25 A $g^{-1}$ presented in Figure 6B reveals that after 1000 cycles, the hybrid capacitor displayed a discharge capacity of 55 mAh $g^{-1}$, corresponding to a 80% capacity retention. The coulombic efficiency of the hybrid capacitor reached ≈98 % after the second cycle.

## 4. CONCLUSION

In conclusion, Na-TNT was originally adopted as negative material for a new energy device, a sodium-ion capacitor, in which an AC positive electrode and a Na-TNT negative electrode were well matched. This new sodium-ion capacitor stands for a very appealing energy-storage device. We can draw the conclusion that the energy density of the AC/Na-TNT sodium-ion capacitor (34 Wh $kg^{-1}$) is comparable to that of an AC/$Li_4Ti_5O_{12}$ lithium-ion hybrid capacitor (30−60 Wh $kg^{-1}$) and is higher than that of an AC/AC double-layer capacitor (26 Wh $kg^{-1}$). Finally, the capacity retention and the long cycling life of AC/Na-TNT capacitor at high rates are also desirable. It is widely acknowledged that the breakthroughs in material science open new horizons for new energy storage and


dx.doi.org/10.1021/am300385r | ACS Appl. Mater. Interfaces 2012, 4, 2762−2768

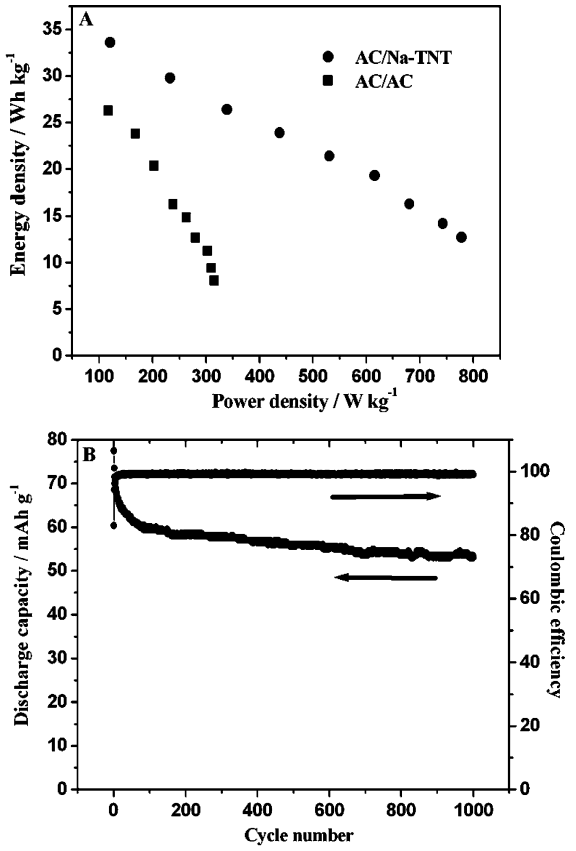


**Figure 6.** (A) Ragone plots of energy density versus power density for AC/Na-TNT and AC/AC capacitors. (B) Long cycling performance and coulombic efficiency of AC/Na-TNT capacitor at a current density of 0.25 A $g^{-1}$.

conversion devices. In this aspect, the AC/Na-TNT sodium-ion hybrid electrochemical capacitor is expected to be as a potential candidate for Na-based energy storage devices. More importantly, the conception of sodium-ion capacitor has been put forward.

## ■ ASSOCIATED CONTENT

### Supporting Information

Experiments, the initial charge−discharge curves for calcined samples with different pH values, long cycling performance of bulk $Na_2Ti_3O_7$ and $Na_2Ti_6O_{13}$, long cycling performance of calcined samples (pH value of 8). This material is available free of charge via the Internet at http://pubs.acs.org.

## ■ AUTHOR INFORMATION

### Corresponding Author

*Phone/Fax: 86-431-85262287. E-mail: hongyuwang@ciac.jl.cn.

### Notes

The authors declare no competing financial interest.

## ■ ACKNOWLEDGMENTS

This project was supported by National Basic Research Program of China (2011CB935702) and Hundred Talents Program of Chinese Academy of Sciences.

## ■ REFERENCES

(1) Yu, G.; Hu, L.; Vosgueritchian, M.; Wang, H.; Xie, X.; Mcdonough, J. R.; Cui, X.; Cui, Y.; Bao, Z. N. *Nano Lett.* **2011**, *11*, 2905.
(2) Zhu, H.; Wang, X. L.; Yang, F.; Yang, X. R. *Adv. Mater.* **2011**, *23*, 2745.
(3) Chen, P. C.; Shen, G. Z.; Shi, Y.; Chen, H.; Zhou, C. W. *ACS Nano* **2010**, *4*, 4403.
(4) An, K. H.; Kim, W. S.; Park, Y. S.; Choi, Y. C.; Lee, S. M.; Chung, D. C.; Bae, D. J.; Lim, S. C.; Lee, Y. H. *Adv. Mater.* **2001**, *13*, 497.
(5) Amatucci, G.; Badway, F.; Pasquier, Du. A.; Zheng, T. *J. Electrochem. Soc.* **2001**, *148*, A 930.
(6) Pell, W. G.; Conway, B. E. *J. Power Sources* **2004**, *136*, 334.
(7) Sikha, G.; Popov, B. N. *J. Power Sources* **2004**, *134*, 130.
(8) Wang, H.; Yoshio, M.; Thapa, A. K.; Nakamura, H. *J. Power Sources* **2007**, *169*, 375.
(9) Wang, Q.; Wen, Z. H.; Li, J. H. *Adv. Funct. Mater.* **2006**, *16*, 2141.
(10) Brousse, T.; Marchand, R.; Taberna, P. L.; Simon, P. *J. Power Sources* **2006**, *158*, 571.
(11) Doeff, M. M.; Ma, Y.; Visco, S. J.; DeJonghe, L. C. *J. Electrochem. Soc.* **1993**, *140*, L169.
(12) Cao, Y.; Xiao, L.; Wang, W.; Choi, D.; Nie, Z.; Yu, J.; Saraf, L. V.; Yang, Z.; Liu, J. *Adv. Mater.* **2011**, *23*, 3155.
(13) Yamada, Y.; Doi, T.; Tanaka, I.; Okada, S. *J. Power Sources* **2011**, *196*, 4837.
(14) Liu, H. M.; Zhou, H. S.; Chen, L. P.; Tang, Z. F.; Yang, W. S. *J. Power Sources* **2011**, *196*, 814.
(15) Kim, D.; Kang, S. H.; Slater, M.; Rood, S.; Vaughey, J. T.; Karan, N.; Balasubramanian, M.; Johnson, C. S. *Adv. Energy Mater.* **2011**, *1*, 333.
(16) Kim, J. S.; Ahn, H. J.; Ryu, H. S.; Kim, D. J.; Cho, G. B.; Kim, K. W.; Nam, T. H. *J. Power Sources* **2008**, *178*, 852.
(17) Zhuo, H. T.; Wang, X. Y.; Tang, A. P.; Liu, Z. M.; Gamboa, S.; Sebastian, P. J. *J/ Power Sources* **2006**, *160*, 698.
(18) Whitacre, J. F.; Tevar, A.; Sharma, S. *Electrochem. Commun.* **2010**, *12*, 463.
(19) Chevrier, V. L.; Ceder, G. *J. Electrochem. Soc.* **2011**, *158*, A1011.
(20) Ong, S. P.; Chevrier, V. L.; Hautier, G.; Jain, A.; Ceder, G. *Energy. Environ. Sci.* **2011**, *4*, 3680.
(21) Senguttuvan, P.; Rousse, G.; Seznec, V.; Tarascon. *J. Chem. Mater.* **2011**, *23*, 4109.
(22) Ge, P.; Fouletier, M. *Solid State Ionics* **1988**, *28*, 1172.
(23) Stevens, D. A.; Dahn, J. R. *J. Electrochem. Soc.* **2001**, *148*, A803.
(24) Asher, R. C. *J. Inorg. Nucl. Chem.* **1959**, *10*, 238.
(25) Wenzel, S.; Hara, T.; Janek, J.; Adelhelm, P. *Energy Environ. Sci.* **2011**, *4*, 3342.
(26) Alcantara, R.; Jimenez, J. M.; Tiradoz, J. L. *J. Electrochem. Soc.* **2002**, *149*, A201.
(27) Stevens, D. A.; Dahn, J. R. *J. Electrochem. Soc.* **2000**, *147*, 1271.
(28) Simon, P.; Gogotsi, Y. *Nature Mater.* **2008**, *7*, 845.
(29) Wang, J.; Polleux, J.; Lim, J.; Dunn, B. *J. Phys. Chem. C* **2007**, *111*, 14925.
(30) Arico, A. S.; Bruce, P.; Scrosati, B.; Tarascon, J. M.; Schalkwijk, W. V. *Nature Mater.* **2005**, *4*, 366.
(31) Bavykin, D. V.; Parmon, V. N.; Lapkin, A. A.; Walsh, F. C. *J. Mater. Chem.* **2004**, *14*, 3370.
(32) (a) Wang, G.; Wang, Q.; Lu, W.; Li, J. *J. Phys. Chem. B* **2006**, *110*, 22029. (b) Chen, Q.; Zhou, W. Z.; Du, G. H.; Peng, M. *Adv. Mater.* **2002**, *14*, 1208.
(33) Riss, A.; Elser, M. J.; Bernardi, J.; Diwald, O. *J. Am. Chem. Soc.* **2009**, *131*, 6198.
(34) Thapa, A. K.; Park, G.; Nakamura, H.; Ishihara, T.; Wang, H.; Yoshio, M. *Electrochim. Acta* **2010**, *55*, 7305.
(35) Jr, E. M.; Abreu, M.; Pravia, O. R. C.; Marinkovic, B. A.; Jardim, P. M.; Rizzo, F. C.; Araujo, A. S. *Solid State Sci.* **2006**, *8*, 888.
(36) Qamar, M.; Yoon, C. R.; Oh, H. J.; Kim, D. H.; Jho, J. H.; Lee, K. S.; Lee, W. J.; Lee, H. G.; Kim, S. J. *Nanotechnology* **2006**, *17*, 5922.
(37) Liu, H.; Yang, D.; Zheng, Z.; Ke, X.; Waclawik, E.; Zhu, H.; Frost, R. L. *J. Raman Spectrosc.* **2010**, *41*, 1331.

(38) Beuvier, T.; Plouet, M. R.; Brohan, L. A. *J. Phys. Chem. C* **2010**, *114*, 7660.
(39) Kolenko, Y. V.; Kovnir, K. A.; Gavrilov, A. I.; Tendeloo, O. G.; Yoshimura, M. *J. Phys. Chem. B* **2006**, *110*, 4030.
(40) Lee, C. K.; Wang, C. C.; Lyu, M. D.; Juang, L. C.; Liu, S. S.; Hung, S. H. *J. Colloid Interface Sci.* **2007**, *316*, 562.
(41) Li, J. L.; Gao, F. *J. Power Sources* **2009**, *194*, 1184.
(42) Wang, H.; Yoshio, M. *J. Power Sources* **2008**, *177*, 681.